Hydrogen-Evolution Reaction in Two-Dimensional PdS_2 by Phase and Defect Engineering

Rafael O. Figueiredo[1,2] and Leandro Seixas[1,2,*]

[1] *MackGraphe—Graphene and Nanomaterials Research Center, Mackenzie Presbyterian University, São Paulo 01302-907, SP, Brazil*

[2] *School of Engineering, Mackenzie Presbyterian University, São Paulo 01302-907, SP, Brazil*

(Received 1 October 2021; revised 19 February 2022; accepted 23 February 2022; published 11 March 2022)

The hydrogen-evolution reaction is an essential step in the electrochemical production of hydrogen without the emission of greenhouse gases. For this reaction, alternative catalyst materials that can replace the platinum of current catalysts are needed. Recent alternatives include two-dimensional materials such as transition metal dichalcogenides. Here, we show the electronic and electrochemical properties of the two-dimensional material palladium disulfide (PdS_2) with two crystal structures (phases) and the formation of native point defects. We analyze the differences between the pentagonal (P-PdS_2) phase and the octahedral ($1T$-PdS_2) phase, point defects and the Gibbs free energies for hydrogen adsorption from first-principles calculations. Our results show that the $1T$-PdS_2 phase has better catalytic activity than the P-PdS_2 phase in the pristine basal plane. In addition, the point defects of lower formation energy in the $1T$-PdS_2 phase, the S vacancies, further improve the catalytic activity for hydrogen production.

DOI: 10.1103/PhysRevApplied.17.034035

I. INTRODUCTION

Since the discovery of graphene in 2004 [1,2], dozens of other two-dimensional (2D) materials have been discovered, with varied electronic, optical, and chemical properties. Among these 2D materials, some of the most promising technological applications are transition metal dichalcogenides (TMDs) [3]. In this class, transition metals form chemical bonds with chalcogens (S, Se, Te), with crystal fields that are usually hexagonal prismatic ($2H$) or octahedral ($1T$). The most well-known TMD, MoS_2, has the $2H$-MoS_2 crystal structure as the one with the lowest energy [3,4]. The bulk is a lamellar material that can be mechanically exfoliated to obtain two-dimensional crystals. Another way to get MoS_2 monolayers is through chemical exfoliation [5]. In this method, Li^+ ions are intercalated between the layers of MoS_2, facilitating the exfoliation by ultrasound. However, there is a charge transfer in the lithiation process, which induces a phase transition in the MoS_2, from $2H$ to $1T$ phase [6]. These phases have very different physical and chemical properties. The material $2H$-MoS_2 is a direct band-gap semiconductor of approximately 2.0 eV [7], while $1T$-MoS_2 is a metal [8].

Recently, MoS_2 has been studied due to its catalytic properties. Although the basal plane of $2H$-MoS_2 is inert to the hydrogen-evolution reaction (HER), the edges of the $2H$-MoS_2 monolayers are chemically active [9,10]. It was also observed that native point defects, such as S vacancies, significantly increase the kinetics of HER in the basal plane [11]. The $1T$-MoS_2 phase also has excellent catalytic activity for the hydrogen-evolution reaction and the metallic characteristic that helps in the electron transfer of the reaction [8,12]. The search for a catalyst for the hydrogen-evolution reaction has recently become very useful for producing molecular hydrogen (H_2) without the emission of greenhouse gases. Today, 95% of hydrogen is made from fossil fuels in steam reforming and coal gasification [13]. This hydrogen is produced for oil refining, ammonia production for fertilizers (Haber-Bosch process) and electric vehicle fuel cells. The production of hydrogen without emission of greenhouse gases (green hydrogen) can be carried out through the electrolysis of water ($2H_2O \rightarrow 2H_2 + O_2$). However, this reaction requires metal catalysts such as platinum (Pt), an expensive and scarce metal. 2D materials like MoS_2 are alternatives to platinum for HER. In this material, the creation of point defects [14], phase transition [8], edges [15], and grain boundaries [16] are ways to control the catalytic activity for hydrogen production.

An exciting and still little explored case is the two-dimensional material palladium dichalcogenide (PdX_2, X = S, Se). The palladium diselenide ($PdSe_2$) has a unique crystal structure, which differs significantly from other TMDs. The $PdSe_2$ monolayer has a Cairo pentagonal tiling (P-$PdSe_2$) crystal structure, in which the transition metal (Pd) has an approximately square planar crystal field [17,18]. In 2020, Jakhar *et al.* [19] and Wu *et al.* [20]

*leandro.seixas@mackenzie.br, https://macksim.org/

observed the phase transition from P-$PdSe_2$ to $1T$-$PdSe_2$ through the lithiation process. For $PdSe_2$, both P-$PdSe_2$ and $1T$-$PdSe_2$ phases are indirect band-gap semiconductors. The palladium disulfide (PdS_2) also has a Cairo pentagonal tiling crystal structure and it is also expected that there will be a phase transition from P-PdS_2 to $1T$-PdS_2 lithiation process. However, the difference in electronic and electrochemical properties of the P-PdS_2 and $1T$-PdS_2 phases and the formation of native point defects in these materials is still unexplored.

In this paper, we investigate the electronic, structural, and catalytic properties of the two-dimensional PdS_2 material in two different phases: P-PdS_2 and $1T$-PdS_2. We analyze the formation of native (neutral) point defects, the electronic properties of these defects, and their effects on the catalytic activity for the hydrogen-evolution reaction. Just as the formation of point defects and phase transitions in MoS_2 increase the catalytic activity, in PdS_2, the pentagonal phase unique to palladium dichalcogenides can result in high activity catalysis unlike anything seen in other 2D materials.

II. METHODS

We perform first-principles atomistic simulations based on the density-functional theory (DFT) [21,22]. The simulations are carried out with the computer code SIESTA [23], which implements DFT on strictly localized basis sets. We use the double-zeta polarized basis set and energy shift of 0.02 eV. In addition, we use exchange-correlation functionals on the Perdew-Burke-Ernzerhof (PBE) approximation [24], norm-conserved pseudopotentials with Troullier-Martins parameterization [25], and mesh cutoff of 400 eV. For simulations of native point defects and hydrogen adsorption, we use $4 \times 4 \times 1$ supercells from the primitive cell for P-PdS_2 and $4 \times 4 \times 1$ supercells from the orthogonalized unit cell [dashed red line in Fig. 1(c)] for $1T$-PdS_2. The k points in the Brillouin zone are sampled with the Monkhorst-Pack algorithm [26] with grid $5 \times 5 \times 1$ for the supercells. For the density of states calculations, we use Gaussian smearing of 0.04 eV and a finer k-point grid of $200 \times 200 \times 1$. All geometries are relaxed entirely until the convergence of forces less than 0.01 eV/Å. All simulations are performed with collinear spin polarization.

The formation energies of point defects [27,28] are calculated from the following equation:

$$\Delta E_f(X) = E_{\text{tot}}(\text{PdS}_2 + X) - E_{\text{tot}}(\text{PdS}_2) + n_{\text{Pd}}\mu_{\text{Pd}} + n_{\text{S}}\mu_{\text{S}}, \quad (1)$$

where $E_{\text{tot}}(X)$ is the total energy of the system X, μ_{Pd} and μ_{S} are the chemical potentials of Pd and S, and n_{Pd} and n_{S} are the variations in the number of Pd and S in the formation of the defect. The chemical potentials of Pd and S are calculated in a scenario rich in Pd (S poor), and rich in S (S rich). In the first scenario, the chemical potential μ_{Pd} is calculated from the total energy of the Pd bulk:

$$\mu_{\text{Pd}}^{\text{S poor}} = E_{\text{tot}}(\text{Pd}), \quad (2)$$

and the chemical potential μ_{S} is calculated using the total energy of P-PdS_2 primitive cell (2 Pd and 4 S per primitive cell):

$$\mu_{\text{S}}^{\text{S poor}} = \frac{E_{\text{tot}}(\text{PdS}_2) - 2\mu_{\text{Pd}}^{\text{S poor}}}{4}. \quad (3)$$

In the second scenario, the chemical potential μ_{S} is calculated through the total energy of the S_8 molecule that forms the sulfur bulk:

$$\mu_{\text{S}}^{\text{S rich}} = \frac{E_{\text{tot}}(\text{S}_8)}{8}, \quad (4)$$

and the chemical potential μ_{Pd} is calculated from the total energy of the PdS_2 primitive cell:

$$\mu_{\text{Pd}}^{\text{S rich}} = \frac{E_{\text{tot}}(\text{PdS}_2) - 4\mu_{\text{S}}^{\text{S rich}}}{2}. \quad (5)$$

The variation in the chemical potential μ_{S} in these two scenarios is

$$\Delta\mu_{\text{S}} = \mu_{\text{S}}^{\text{S rich}} - \mu_{\text{S}}^{\text{S poor}} = 0.726 \text{ eV}. \quad (6)$$

For the investigation of the catalytic activity of the material for HER, Gibbs free energies for hydrogen adsorption are calculated:

$$\Delta G_{\text{H}} = E_{\text{tot}}(X + H) - E_{\text{tot}}(X) - \mu_{\text{H}} + \Delta E_{\text{ZPE}} - T\Delta S_{\text{H}}, \quad (7)$$

where ΔS_{H} is the entropy variation from the H adsorbed to the H in the H_2 molecule, T is the temperature, ΔE_{ZPE} is the variation of the zero-point energy (ZPE) by the adsorption of H. The entropy change of the adsorbed hydrogen is calculated as $T\Delta S_{\text{H}} \approx -(1/2)T\Delta S_{\text{H}_2}$, where ΔS_{H_2} is the entropy of the H_2 gas given by the NIST-JANAF thermochemical tables [29]. At $T = 300$ K, this term is $(1/2)T\Delta S_{\text{H}_2} = 0.203$ eV. The ZPE variation is calculated for hydrogens adsorbed in the $1T$-PdS_2 and P-PdS_2 phases, compared to the ZPE of the H_2 molecule. For P-PdS_2 this variation is $\Delta E_{\text{ZPE}} = 0.040$ eV and for $1T$-PdS_2 the variation is $\Delta E_{\text{ZPE}} = 0.036$ eV. We note that we can do the Nørskov approximation [30], in which the term $\Delta E_{\text{ZPE}} - T\Delta S_{\text{H}}$ can be approximated by a constant:

$$\Delta G_{\text{H}} = E_{\text{tot}}(X + H) - E_{\text{tot}}(X) - \mu_{\text{H}} + 0.24 \text{ eV}. \quad (8)$$

We expect that this variation of ZPE between materials, less than 0.01 eV, will also be maintained for materials with native defects.

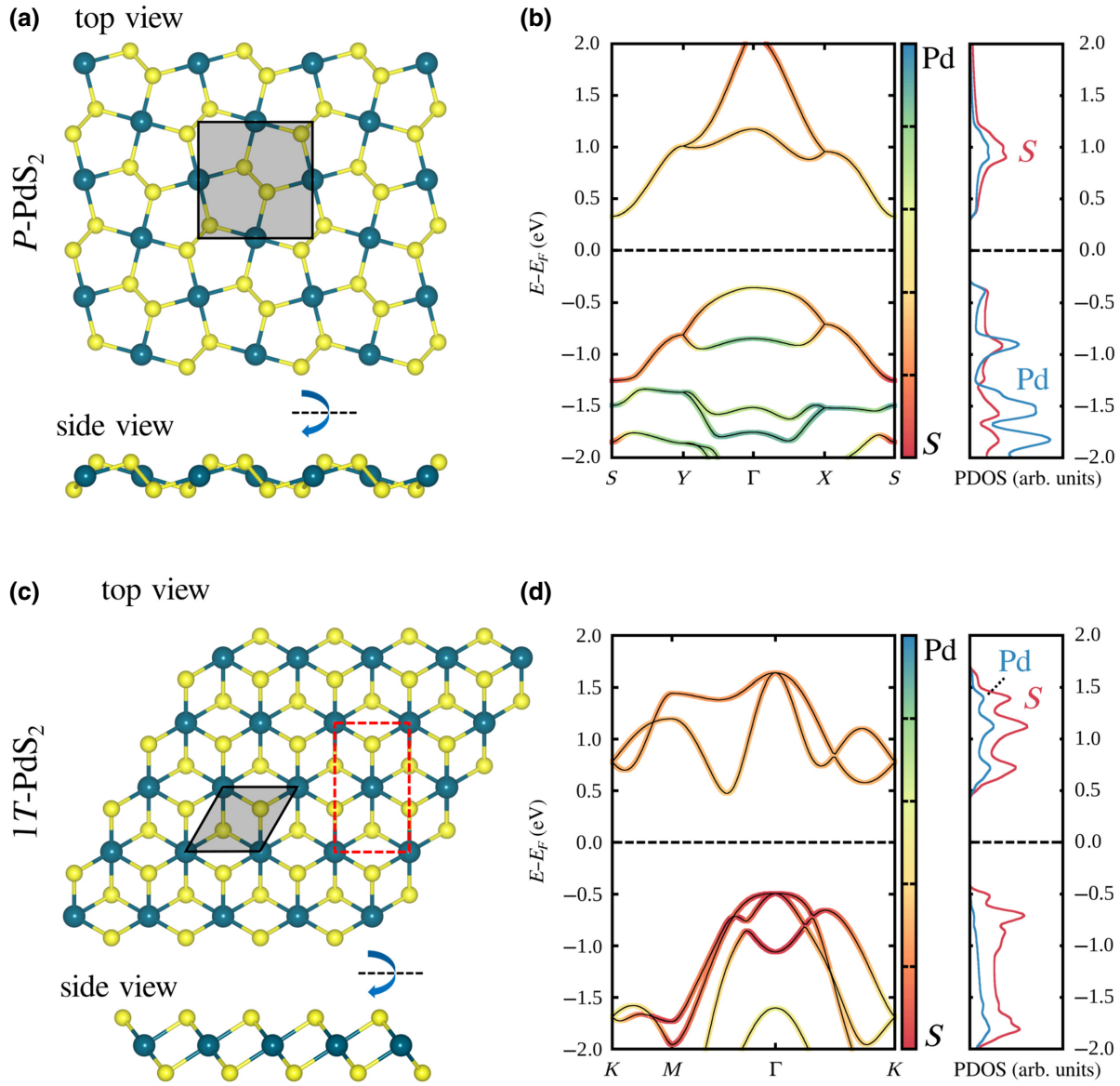

FIG. 1. Structural and electronic properties of PdS_2. (a) Ball-and-stick representation of P-PdS_2. (b) Electronic band structure and projected density of states of P-PdS_2. (c) Ball-and-stick representation of $1T$-PdS_2. (d) Electronic band structure and projected density of states of $1T$-PdS_2. Primitive unit cells are shown by the black line, and orthogonalized unit cells by the dashed red line. The Fermi levels in (b),(d) are shown as dashed black lines.

III. RESULTS AND DISCUSSION

The two-dimensional palladium disulfide in this work is studied in the P-PdS_2 and $1T$-PdS_2 phases, as shown in Fig. 1. The P-PdS_2 phase has lower energy than the $1T$-PdS_2, with $\Delta E = E_{1T} - E_P = 0.343$ eV/(formula unit). The P-PdS_2 phase has an orthorhombic unit cell with lattice constants $a = 5.608$ Å and $b = 5.717$ Å. The $1T$-PdS_2 phase has a trigonal unit cell with and lattice constant $a = 3.609$ Å, this is greater than the 3.068 Å of Ref. [31]. This difference is mainly due to the exchange-correlation functional with correction of the van der Waals interaction and the difference in the DFT implementation method. Both phases are semiconductor with indirect band gap, depicted in Figs. 1(b) and 1(d). The contributions of the Pd atomic orbitals in the Bloch states are shown through the color map in the bands, with blue for Bloch states with more significant contributions from the Pd orbitals. Figure 1 also shows the projected density of states (PDOS) normalized by the number of atoms. Although both phases are indirect band-gap semiconductors, the band structures are entirely different. The P-PdS_2 valence band has an enormous contribution from the Pd orbitals. In comparison, the $1T$-PdS_2 valence band has a significant contribution from the S. It is expected that the formation of native

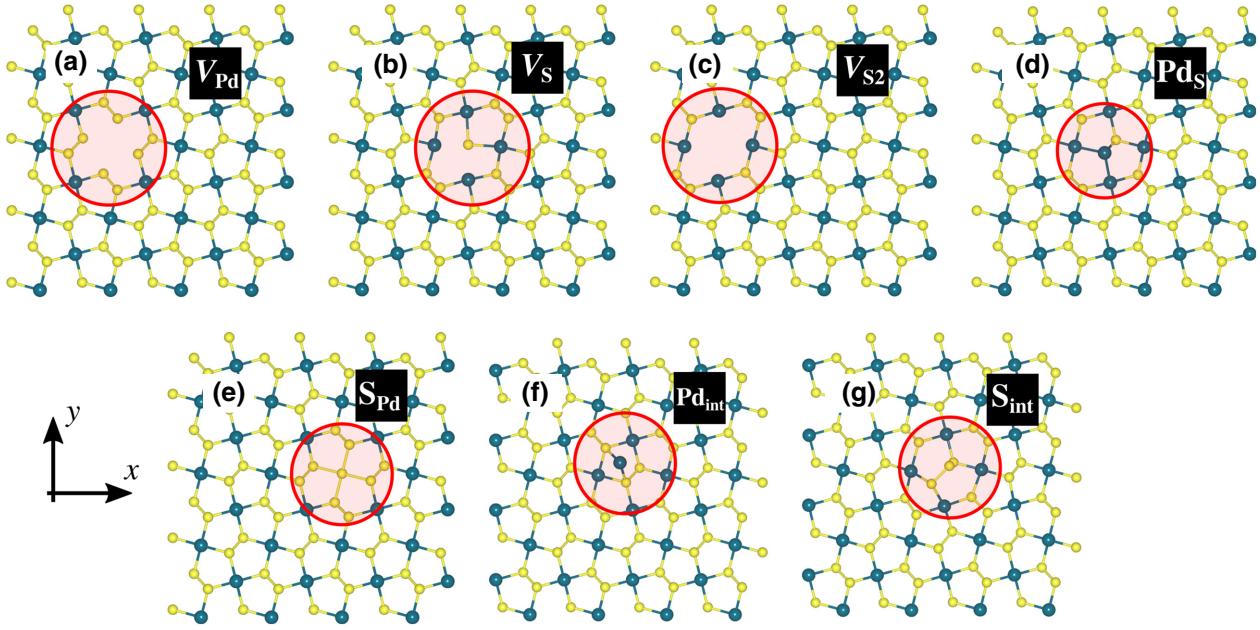

FIG. 2. Geometry of native point defects of P-PdS_2: (a) V_{Pd}, (b) V_S, (c) V_{S2}, (d) Pd_S, (e) S_{Pd}, (f) Pd_{int}, (g) S_{int}. The defect region is highlighted by the red circle.

point defects has different effects between these materials. Effects of spin-orbit coupling (SOC) on band structures are shown in Fig. S1 within the Supplemental Material [32]. The SOC effect of PdS_2 is much smaller than the platinum dichalcogenides shown in Ref. [33].

For the P-PdS_2 phase, native point defects formed by vacancies (V_{Pd}, V_S, V_{S2}), substitutional (Pd_S, S_{Pd}) and interstitial (Pd_{int}, S_{int}) defects are investigated. The reconstruction of the geometries of these specific defects is shown in Fig. 2. The red circle in the figure highlights the defect region. There are few local distortions in the crystal lattice around the defect. For phase $1T$-PdS_2, we investigate specific defects formed by vacancies (V_{Pd}, V_S), substitutional (Pd_S, S_{Pd}) and interstitial (Pd_{int}, S_{int}) defects, depicted in Fig. 3. As in the P-PdS_2 phase, there are small effects of reconstructions of the geometry around the defect, highlighted by the red circle.

The formation energies of these defects are studied in scenarios rich in Pd (S poor) and rich in S (S rich). In these scenarios, the chemical potentials μ_{Pd} and μ_S vary

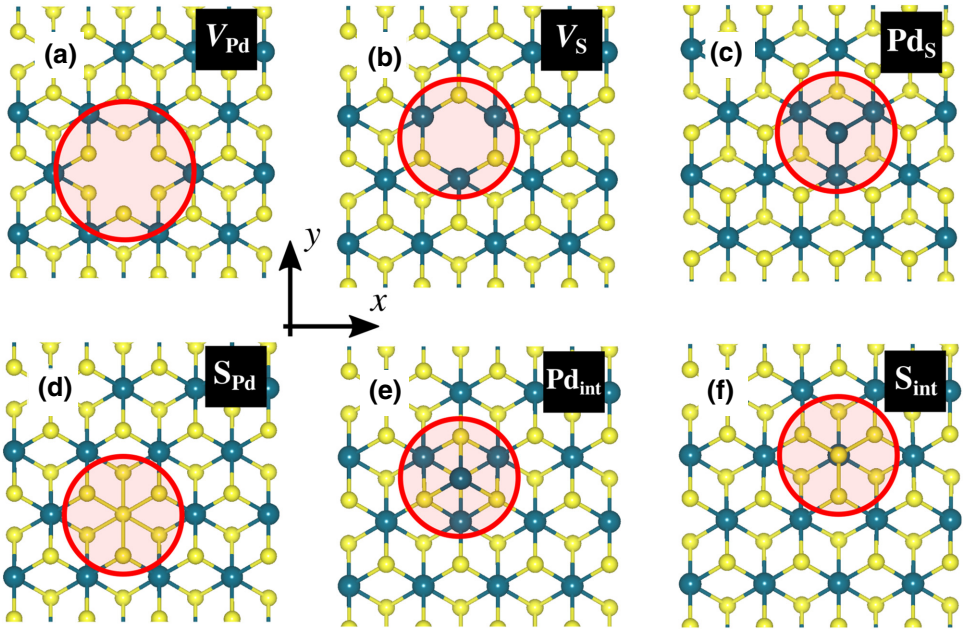

FIG. 3. Geometry of native point defects of $1T$-PdS_2: (a) V_{Pd}, (b) V_S, (c) Pd_S, (d) S_{Pd}, (e) Pd_{int}, (f) S_{int}. The defect region is highlighted by the red circle. The point defect is created in a $4 \times 4 \times 1$ supercell of the orthogonal unit cell shown in Fig. 1.

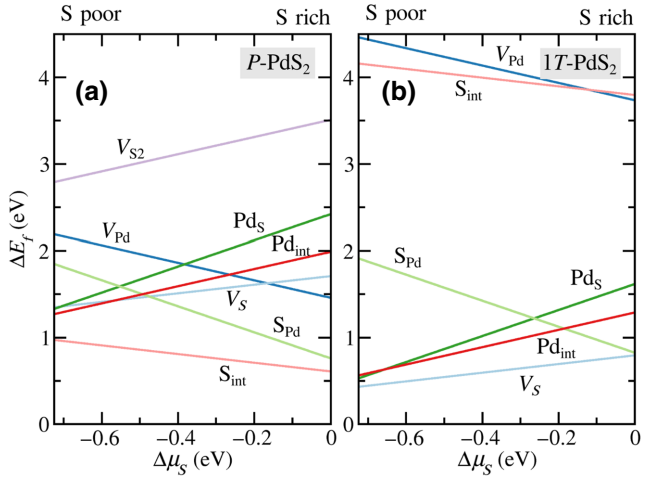

FIG. 4. Defect formation energy: (a) P-PdS_2, (b) $1T$-PdS_2. The defect formation energies are calculated for neutral defects.

according to the abundance of the elements Pd and S. The values of these chemical potentials are calculated as shown in Sec. II.

The formation energies of the native (neutral) point defects in the P-PdS_2 phase are shown in Fig. 4(a), whereas the $1T$-PdS_2 phase are shown in Fig. 4(b). We notice that the minor formation energies (most abundant defects) in the two phases are quite different. In the P-PdS_2 phase, the S_{int} defect is the one with the lowest energy (most abundant) for the entire range of the sulfur chemical potential. The second-lowest energy defect varies according to the chemical potential μ_S, with the S_{Pd} defect being the second lowest energy in the S-rich scenario, and the Pd_{int} defect for the S-poor scenario. In $1T$-PdS_2 phase, the lowest energy for the point defect is a sulfur vacancy (V_S), for the entire region of chemical potential μ_S. The second most common defect (second-lowest energy) varies according to the chemical potential, with Pd_{int} being more common in the S-poor scenario, and S_{Pd} in the S-rich scenario. It is worthwhile to note that while the S_{int} defect is the one with the lowest formation energy for the P-PdS_2 material, it is one of the highest energies for the $1T$-PdS_2.

The electronic properties of the P-PdS_2 and $1T$-PdS_2 with point defects are shown through the PDOS, depicted in Figs. 5 and 6, respectively. The electronic states projected on the S atomic orbitals are shown in orange, and those projected on the Pd orbitals are shown in green. We notice that the V_{Pd} defect in P-PdS_2 doped the material with electron acceptors (p-type doping), while the other point defects in P-PdS_2 introduce deep impurity levels. In addition, the V_{S2} defect raises two levels located in the middle of the band gap, one filled and one empty. In this material, the V_S and Pd_S defects create peaks in the PDOS close to the conduction band. The Pd_{int} defect creates a peak close to the valence band. For point defects in $1T$-PdS_2, we note that V_S, S_{Pd}, Pd_{int}, and S_{int} defects introduce levels located in the middle of the band gap. Adsorption of impurities in these defects must transfer charge filling and emptying these localized levels, changing the electronic properties drastically. For the density of states of P-PdS_2 and $1T$-PdS_2 with defects and hydrogen adsorbed, see Fig. S2 and S3 within the Supplemental Material [32].

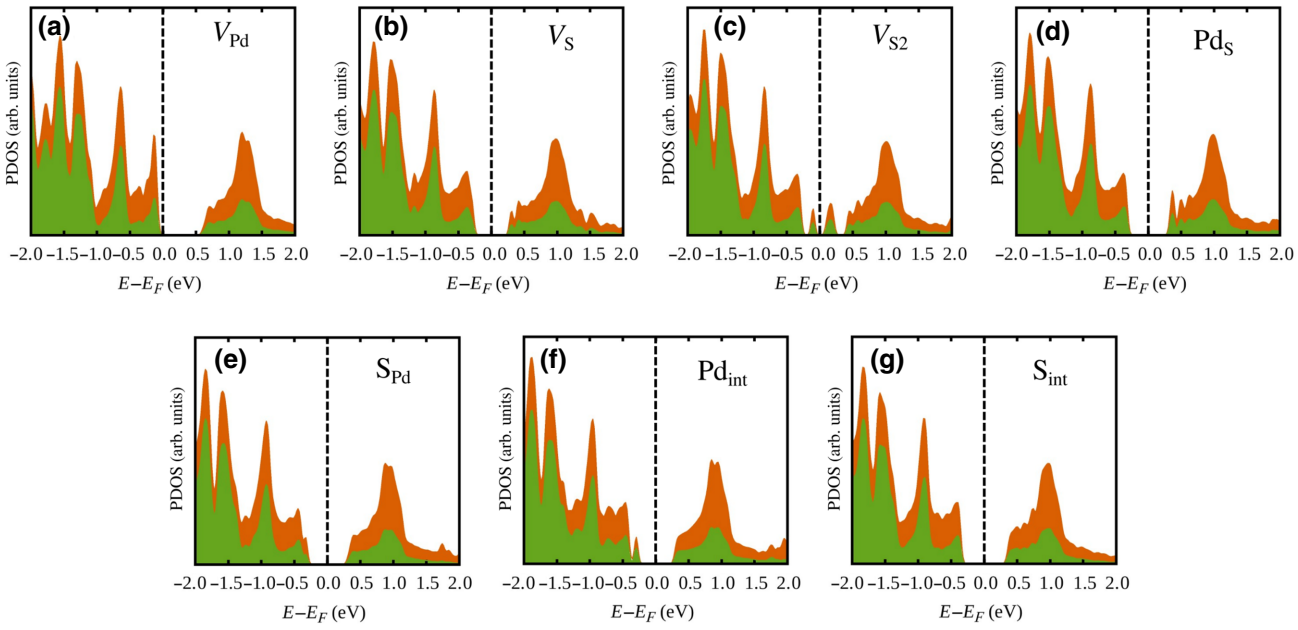

FIG. 5. Projected density of states for P-PdS_2 with defects: (a) V_{Pd}, (b) V_S, (c) V_{S2}, (d) Pd_S, (e) S_{Pd}, (f) Pd_{int}, (g) S_{int}. The green (orange) area represents Pd (S) electronic states. The Fermi levels are shown as dashed black lines.

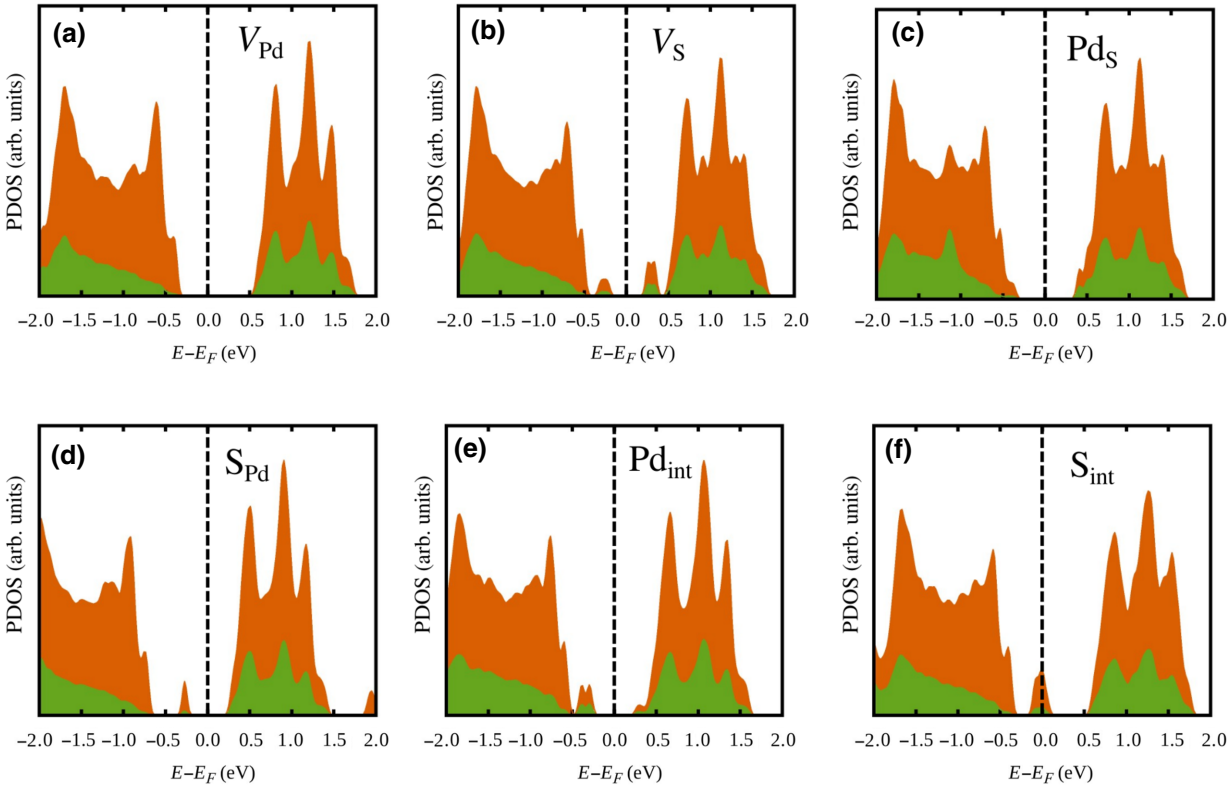

FIG. 6. Projected density of states for 1T-PdS_2 with defects: (a) V_{Pd}, (b) V_S, (c) Pd_S, (d) S_{Pd}, (e) Pd_{int}, (f) S_{int}. The green (orange) area represents Pd (S) electronic states. The Fermi levels are shown as dashed black lines.

The two most common defects of P-PdS_2 in the S-rich scenario, S_{int} and S_{Pd}, slightly alter the electronic properties of the material. Meanwhile, the most common point defects of 1T-PdS_2, V_S and S_{Pd} cause more significant changes in electronic properties, with the appearance of levels located in the middle of the gap. We observe at least three peaks in the PDOS of the V_S defect in 1T-PdS_2, with a filled state and two empty states; and at least one localized filled state in the PDOS of the S_{Pd} in 1T-PdS_2.

As well as the generation of point defects in MoS_2 increasing the catalytic activity of the basal plane for HER, it is also expected that defects in PdS_2 may increase catalytic activity when compared to pristine materials. For pristine materials, Gibbs free energies are 1.22 eV for P-PdS_2 and 0.55 eV for 1T-PdS_2. These Gibbs free energies are calculated in a dilute adsorbed hydrogen regime. Defects in PdS_2 alter these free Gibbs energies, as shown in Fig. 7. For the P-PdS_2 phase the V_{Pd} and V_S defects decrease ΔG_H to −0.19 eV, the V_{S2} defect to 0.45 eV, Pd_S decreases to 0.46 eV, S_{Pd} decreases to 0.66 eV, S_{int} to 0.71 eV, and finally, the Pd_{int} defect decreases the ΔG_H to 1.17 eV. All point defects increase the catalytic activity for HER. For the 1T-PdS_2 phase, the point defect that optimizes the catalytic activity for HER is the vacancy of S (V_S), which decreases the ΔG_H to 0.30 eV. The other defects of 1T-PdS_2 change the ΔG_H as follows: Pd_S decreases to 0.34 eV, S_{Pd} decreases to 0.55 eV, Pd_{int} increases ΔG_H to 0.68 eV, V_{Pd} changes to −1.01 eV, and S_{int} changes to −3.37 eV. Unlike P-PdS_2 phase, in 1T-PdS_2 phase there are point defects that improve (V_S, Pd_S, S_{Pd}), and defects that worsen (Pd_{int}, S_{int}, V_{Pd}) the catalytic activity.

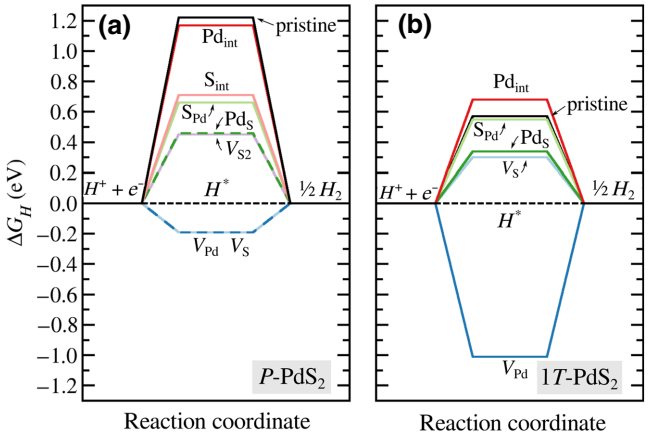

FIG. 7. Gibbs free energy diagram for hydrogen adsorption. (a) Native defects in P-PdS_2. (b) Native defects in 1T-PdS_2. Optimal catalytic activity is achieved at $\Delta G_H = 0$.

It is worthwhile to note the relationship of the most common point defects (lower formation energies) and their catalytic activities (lower $|\Delta G_H|$). In the P-PdS_2 phase, the most abundant defects (S_{int}, S_{Pd}) have a ΔG_H of approximately 0.7 eV, which is better than the basal plane of the pristine material ($\Delta G_H = 1.22$ eV). In phase $1T$-PdS_2 the most common defect (V_S) is also the one that best optimizes the catalytic activity, $\Delta G_H = 0.30$ eV. Therefore, $1T$-PdS_2 with relevant concentrations of point defects is expected to have excellent catalytic activity for the hydrogen-evolution reaction.

Finally, we analyze the evolution of the crystal structure of the P-PdS_2 and $1T$-PdS_2 (pristine) with the adsorption of several hydrogen atoms. The Gibbs free energies vary widely with the number of H adsorbed. In P-PdS_2, it varies from 1.22 to -1.42 eV, for 1 and 27 hydrogens adsorbed on the 4×4 supercell. In $1T$-PdS_2, it varies from 0.57 to -0.53 eV, for 1 and 28 hydrogens adsorbed on the orthogonalized 4×4 supercell. This considerable variation is caused by the formation of complex structural defects with the adsorption of H, as shown in Fig. 8. When we increase H adsorbed in the basal plane, the number of complex defects increases. These defects are difficult to associate with those shown in Figs. 2 and 3. This number of adsorbed atoms can be controlled by the partial pressure of the acid solution in which the catalyst is immersed. It can also be tuned for optimization of catalytic activity and phase engineering, and point defect formation.

The phase engineering and formation of defects in PdS_2 can be compared with another two-dimensional material from the group of transition metal dichalcogenides, the MoS_2. For MoS_2, a $2H$ to $1T'$ phase transition occurs with the Li^+ ion intercalation process. The $2H$-MoS_2 phase is inert to HER ($\Delta G_H = 2.0$ eV) [14], while the $1T'$-MoS_2 phase is active with a ΔG_H of approximately 0.06 eV [34]. This more abrupt change occurs due to the transition in the electronic properties of MoS_2, from the semiconductor phase ($2H$) the metallic phase ($1T'$). For PdS_2, both P-PdS_2 and $1T$-PdS_2 phases are semiconductor, so we have a slightly smaller change in Gibbs free energies for hydrogen adsorption, from 1.22 eV (P-PdS_2) to 0.57 eV ($1T$-PdS_2). We can compare PdS_2 with point defects with MoS_2 also with point defects. Although the basal plane of pristine $2H$-MoS_2 is inert for HER, native point defects such as

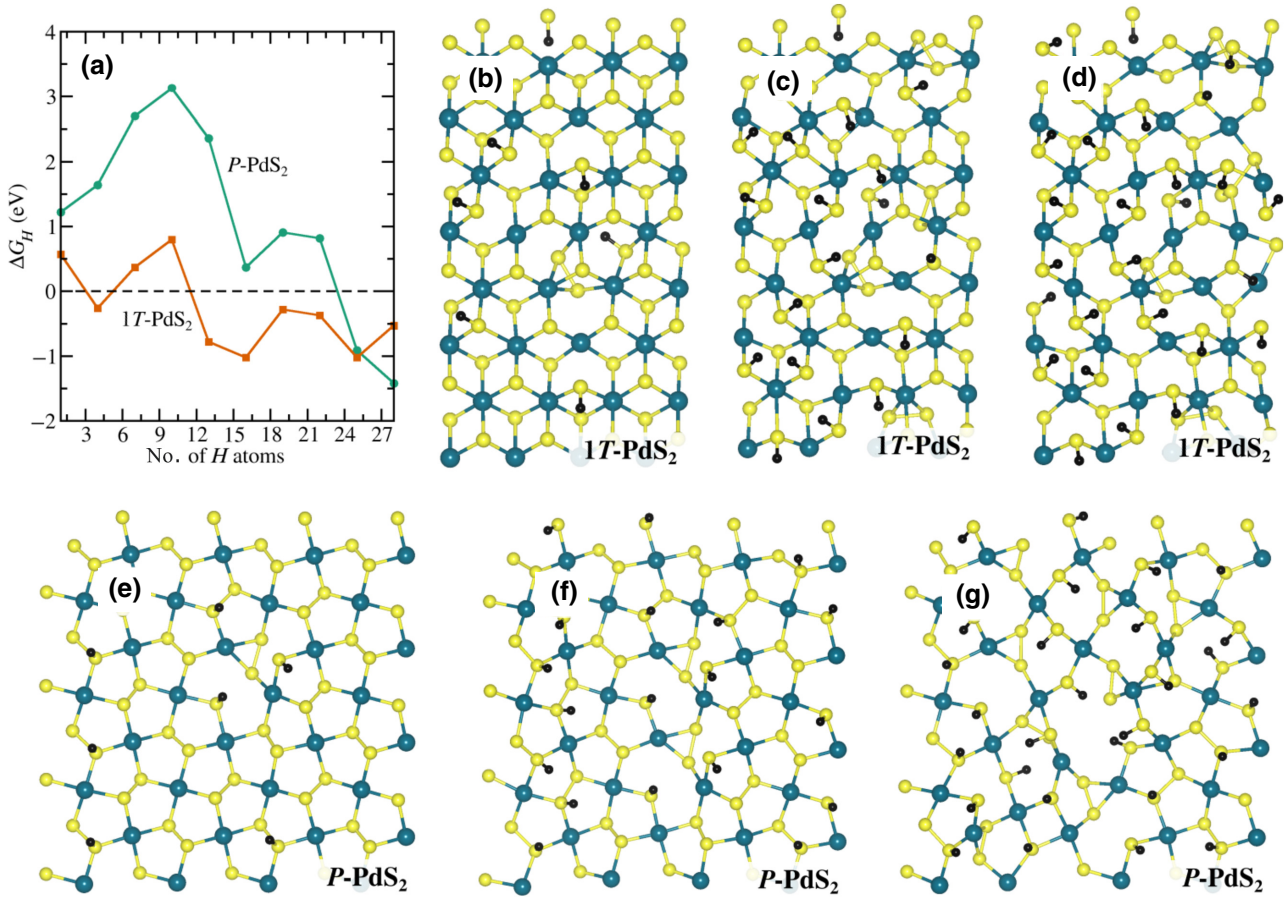

FIG. 8. (a) Gibbs free energy for hydrogen adsorption for pristine P-PdS_2 and $1T$-PdS_2 as a function of the number of H atoms adsorbed. Geometry of $1T$-PdS_2 with (b) 7 H, (c) 19 H, (d) 28 H atoms adsorbed. Geometry of P-PdS_2 with (e) 7 H, (f) 19 H, (g) 28 H. Pd atoms are shown in green, S in yellow, and H in black.

S vacancies in $2H$-MoS_2 significantly decrease the ΔG_H that makes the material a catalyst for this reaction [14]. However, an optimal ΔG_H occurs only with a high concentration of defects (approximately equal to 13% of S vacancies). This high concentration of defects makes it difficult to apply this material for applications in hydrogen synthesis. The P-PdS_2 and $1T$-PdS_2 materials shown here are studied with much lower defect concentrations, such as 1.6% of S vacancies. These low concentrations of defects are easier to form naturally in PdS_2 synthesis or induced by processes such as plasma beams. It should also be noted that the chemical exfoliation of MoS_2, in addition to inducing the $2H$ to $1T'$ phase transition, also creates defects in the basal plane of the material [35]. Thus, we expect that the P-PdS_2 to $1T$-PdS_2 phase transition can also create native defects that increase the catalytic activity for HER. The most common defects would be those with lower formation energy, such as S vacancies, which are also, so that optimize the ΔG_H for the electrochemical production of hydrogen. The $1T$-PdS_2 material obtained through the phase transition by lithiation must contain point defects that will make it an excellent catalyst for the hydrogen-evolution reaction.

We investigate the adsorption of several hydrogen atoms in the basal plane of PdS_2 to determine point defects through the formation of H_2S instead of H_2 [36]. The formation of H_2S could create defects such as sulfur vacancies. In fact, we observe the formation of defects in PdS_2, but not directly related to the formation of S vacancies. The observed defects are more complex and vary the Gibbs free energy in a nononotonic way.

IV. CONCLUSION

The two-dimensional PdS_2 can have its electronic and catalytic properties for HER adjusted through a phase engineering (P-PdS_2 and $1T$-PdS_2) and through the formation of native point defects, i.e., vacancies, substitutional and interstitial defects of elements that make up the material itself (Pd and S). It is found that the basal plane of $1T$-PdS_2 (pristine) has a higher catalytic activity than P-PdS_2, and that native point defects such as V_S, Pd_S, and S_{Pd} can further increase this catalytic activity. The most abundant point defect of $1T$-PdS_2 (lower formation energy) is also the one that best optimizes the hydrogen-evolution reaction. Finally, variations in the basal plane covering with H atoms change the Gibbs free energy drastically due to more complex defects involving hydrogen. In general, the unique crystal structure of the two-dimensional materials that is only found in palladium dichalcogenides (Cairo pentagonal tiling) is more inert to the hydrogen-evolution reaction than the $1T$-PdS_2 crystal structure. However, it is essential to note that monovacancies (V_S and V_{Pd}) are more reactive in P-PdS_2 than in $1T$-PdS_2. The unique crystal structure of PdS_2 (P-PdS_2) differs widely from the $1T$-PdS_2 phase when point defect formations and their consequences on electronic and catalytic properties are analyzed. Two-dimensional palladium dichalcogenides are being recently studied for applications in nanoelectronics [37], solar cells [19], and thermoelectric devices [38]. In this work, we show that an application of these materials can be found when there are point defects or phase transitions, the electrochemical production of green hydrogen.

ACKNOWLEDGMENT

We thank MackPesquisa and CNPq (Grants No. 40825/2018-5 and No. 311324/2020-7) for financial support. We also thank computational facilities provided by the High Performance Computing Center (NACAD) at COPPE/UFRJ.

[1] K. S. Novoselov, A. K. Geim, S. V. Morozov, D. Jiang, Y. Zhang, S. V. Dubonos, I. V. Grigorieva, and A. A. Firsov, Electric field effect in atomically thin carbon films, Science **306**, 666 (2004).

[2] A. H. Castro Neto, F. Guinea, N. M. R. Peres, K. S. Novoselov, and A. K. Geim, The electronic properties of graphene, Rev. Mod. Phys. **81**, 109 (2009).

[3] S. Manzeli, D. Ovchinnikov, D. Pasquier, O. V. Yazyev, and A. Kis, 2D transition metal dichalcogenides, Nat. Rev. Mater. **2**, 17033 (2017).

[4] K. F. Mak, C. Lee, J. Hone, J. Shan, and T. F. Heinz, Atomically Thin MoS_2: A new Direct-Gap Semiconductor, Phys. Rev. Lett. **105**, 136805 (2010).

[5] P. Joensen, R. Frindt, and S. R. Morrison, Single-layer MoS_2, Mater. Res. Bull. **21**, 457 (1986).

[6] D. Nasr Esfahani, O. Leenaerts, H. Sahin, B. Partoens, and F. Peeters, Structural transitions in monolayer MoS_2 by lithium adsorption, J. Phys. Chem. C **119**, 10602 (2015).

[7] J. E. Padilha, H. Peelaers, A. Janotti, and C. G. Van de Walle, Nature and evolution of the band-edge states in MoS_2: From monolayer to bulk, Phys. Rev. B **90**, 205420 (2014).

[8] D. Voiry, M. Salehi, R. Silva, T. Fujita, M. Chen, T. Asefa, V. B. Shenoy, G. Eda, and M. Chhowalla, Conducting MoS_2 nanosheets as catalysts for hydrogen evolution reaction, Nano Lett. **13**, 6222 (2013).

[9] T. F. Jaramillo, K. P. Jørgensen, J. Bonde, J. H. Nielsen, S. Horch, and I. Chorkendorff, Identification of active edge sites for electrochemical H_2 evolution from MoS_2 nanocatalysts, Science **317**, 100 (2007).

[10] S. Li, S. Wang, M. M. Salamone, A. W. Robertson, S. Nayak, H. Kim, S. E. Tsang, M. Pasta, and J. H. Warner, Edge-enriched 2D MoS_2 thin films grown by chemical vapor deposition for enhanced catalytic performance, ACS Catal. **7**, 877 (2017).

[11] L. Li, Z. Qin, L. Ries, S. Hong, T. Michel, J. Yang, C. Salameh, M. Bechelany, P. Miele, and D. Kaplan *et al.*, Role of sulfur vacancies and undercoordinated Mo regions in MoS_2 nanosheets toward the evolution of hydrogen, ACS Nano **13**, 6824 (2019).

[12] D. Voiry, R. Fullon, J. Yang, C. d. C. C. e Silva, R. Kappera, I. Bozkurt, D. Kaplan, M. J. Lagos, P. E. Batson, and G. Gupta *et al.*, The role of electronic coupling between substrate and 2D MoS_2 nanosheets in electrocatalytic production of hydrogen, Nat. Mater. **15**, 1003 (2016).

[13] K. Liu, C. Song, and V. Subramani, *Hydrogen and Syngas Production and Purification Technologies* (John Wiley & Sons, Hoboken, New Jersey, 2010).

[14] H. Li, C. Tsai, A. L. Koh, L. Cai, A. W. Contryman, A. H. Fragapane, J. Zhao, H. S. Han, H. C. Manoharan, and F. Abild-Pedersen *et al.*, Activating and optimizing MoS_2 basal planes for hydrogen evolution through the formation of strained sulphur vacancies, Nat. Mater. **15**, 48 (2016).

[15] B. Mohanty, M. Ghorbani-Asl, S. Kretschmer, A. Ghosh, P. Guha, S. K. Panda, B. Jena, A. V. Krasheninnikov, and B. K. Jena, MoS_2 quantum dots as efficient catalyst materials for the oxygen evolution reaction, ACS Catal. **8**, 1683 (2018).

[16] J. Li, T. Joseph, M. Ghorbani-Asl, S. Kolekar, A. V. Krasheninnikov, and M. Batzill, Mirror twin boundaries in $MoSe_2$ monolayers as one dimensional nanotemplates for selective water adsorption, Nanoscale **13**, 1038 (2021).

[17] C. Soulard, X. Rocquefelte, P.-E. Petit, M. Evain, S. Jobic, J.-P. Itié, P. Munsch, H.-J. Koo, and M.-H. Whangbo, Experimental and theoretical investigation on the relative stability of the PdS_2-and pyrite-type structures of $PdSe_2$, Inorg. Chem. **43**, 1943 (2004).

[18] Y. Wang, Y. Li, and Z. Chen, Not your familiar two dimensional transition metal disulfide: Structural and electronic properties of the PdS_2 monolayer, J. Mater. Chem. C **3**, 9603 (2015).

[19] M. Jakhar, J. Singh, A. Kumar, and R. Pandey, First-principles study of the hexagonal T-phase $PdSe_2$ monolayer and its application in solar cells, J. Phys. Chem. C **124**, 26565 (2020).

[20] Z. Wu, L. Lu, X. Liang, C. Dun, S. Yan, E. Mu, Y. Liu, and Z. Hu, Formation of hexagonal $PdSe_2$ for electronics and catalysis, J. Phys. Chem. C **124**, 10935 (2020).

[21] P. Hohenberg and W. Kohn, Inhomogeneous electron gas, Phys. Rev. **136**, B864 (1964).

[22] W. Kohn and L. J. Sham, Self-consistent equations including exchange and correlation effects, Phys. Rev. **140**, A1133 (1965).

[23] A. García, N. Papior, A. Akhtar, E. Artacho, V. Blum, E. Bosoni, P. Brandimarte, M. Brandbyge, J. Cerdá, and F. Corsetti *et al.*, SIESTA: Recent developments and applications, J. Chem. Phys. **152**, 204108 (2020).

[24] J. P. Perdew, K. Burke, and M. Ernzerhof, Generalized Gradient Approximation Made Simple, Phys. Rev. Lett. **77**, 3865 (1996).

[25] N. Troullier and J. L. Martins, Efficient pseudopotentials for plane-wave calculations, Phys. Rev. B **43**, 1993 (1991).

[26] H. J. Monkhorst and J. D. Pack, Special points for Brillouin-zone integrations, Phys. Rev. B **13**, 5188 (1976).

[27] S. B. Zhang and J. E. Northrup, Chemical Potential Dependence of Defect Formation Energies in GaAs: Application to Ga Self-Diffusion, Phys. Rev. Lett. **67**, 2339 (1991).

[28] C. Freysoldt, B. Grabowski, T. Hickel, J. Neugebauer, G. Kresse, A. Janotti, and C. G. Van de Walle, First-principles calculations for point defects in solids, Rev. Mod. Phys. **86**, 253 (2014).

[29] M. W. Chase Jr., *NIST-JANAF thermochemical tables* (Fourth edition. Washington, DC: American Chemical Society; New York: American Institute of Physics for the National Institute of Standards and Technology, 1998., 1998) issued as: Journal of Physical and Chemical Reference Data; monograph no. 9, 1998.; includes bibliographies.

[30] J. K. Nørskov, T. Bligaard, A. Logadottir, J. Kitchin, J. G. Chen, S. Pandelov, and U. Stimming, Trends in the exchange current for hydrogen evolution, J. Electrochem. Soc. **152**, J23 (2005).

[31] M. Ghorbani-Asl, A. Kuc, P. Miro, and T. Heine, A single-material logical junction based on 2D crystal PdS_2, Adv. Mater. **28**, 853 (2016).

[32] See the Supplemental Material at http://link.aps.org/supplemental/10.1103/PhysRevApplied.17.034035 for details of the band structure of PdS_2 with and witout spin-orbit coupling, and density of states of PdS_2 with defects and hydrogen adsorbed. CIF files of defective crystal structures are also provided.

[33] J. Li, S. Kolekar, M. Ghorbani-Asl, T. Lehnert, J. Biskupek, U. Kaiser, A. V. Krasheninnikov, and M. Batzill, Layer-dependent band gaps of platinum dichalcogenides, ACS Nano **15**, 13249 (2021).

[34] G. Gao, Y. Jiao, F. Ma, Y. Jiao, E. Waclawik, and A. Du, Charge mediated semiconducting-to-metallic phase transition in molybdenum disulfide monolayer and hydrogen evolution reaction in new 1T phase, J. Phys. Chem. C **119**, 13124 (2015).

[35] R. Naz, M. Imtiaz, Q. Liu, L. Yao, W. Abbas, T. Li, I. Zada, Y. Yuan, W. Chen, and J. Gu, Highly defective 1T-MoS_2 nanosheets on 3D reduced graphene oxide networks for supercapacitors, Carbon **152**, 697 (2019).

[36] C. Tsai, H. Li, S. Park, J. Park, H. S. Han, J. K. Nørskov, X. Zheng, and F. Abild-Pedersen, Electrochemical generation of sulfur vacancies in the basal plane of MoS_2 for hydrogen evolution, Nat. Commun. **8**, 1 (2017).

[37] A. D. Oyedele, S. Yang, L. Liang, A. A. Puretzky, K. Wang, J. Zhang, P. Yu, P. R. Pudasaini, A. W. Ghosh, and Z. Liu *et al.*, $PdSe_2$: Pentagonal two-dimensional layers with high air stability for electronics, J. Am. Chem. Soc. **139**, 14090 (2017).

[38] D. Qin, P. Yan, G. Ding, X. Ge, H. Song, and G. Gao, Monolayer $PdSe_2$: A promising two-dimensional thermoelectric material, Sci. Rep. **8**, 1 (2018).